Published on 10 September 2014. Downloaded by Hefei Institutes of Physical Science, Chinese Academy of Sciences on 04/12/2014 00:43:01.

Analyst

PAPER

View Article Online
View Journal | View Issue

Cite this: *Analyst*, 2014, **139**, 5983

Raman scattering and plasmonic photocatalysis of single particles of $NaYF_4$:Yb,Er@Ag under near-infrared laser excitation†

Yongmei Ma, Honglin Liu,* Zhenzhen Han, Liangbao Yang,* Bai Sun and Jinhuai Liu

Received 4th July 2014
Accepted 9th September 2014

DOI: 10.1039/c4an01202j

www.rsc.org/analyst

This study has investigated the plasmonic photocatalytic ability of silver nanoparticles (Ag NPs) and the significantly improved Raman achieved by decorating them on a single $NaYF_4$:Yb,Er upconversion (UC) microcrystal under near-infrared excitation. This points to new applications for UC-noble metal composites and promises a novel method for constructing SERS-active nanostructures.

1. Introduction

Surface-enhanced Raman scattering (SERS), widely used in a number of fields concerned with detective work, can provide excellent fingerprint information with a high degree of sensitivity.[1–3] Its performance depends on a number of factors, in particular a strong reliance on an external excitation light source.[4] It is noted that the excitation lasers in most SERS studies involve UV/visible light[5,6] which can readily be made to match the localized surface plasmon resonance (LSPR) frequency of noble metal nanostructures.[7–10] However, UV/visible light has short sample penetration depths, and high laser power can result in a strong heating effect, and each of these will restrict its use in luminescent stains for bioimaging.[11] In general, a laser of longer wavelength will give much deeper penetration, as for example in near-infrared (NIR) lighting.[12] One has to tune the LSPR features of nanostructures using a complex assembly to match NIR excitation to give high SERS sensitivity.[13,14] There remains a considerable challenge to the construction of nanostructures whose LSPR can readily match NIR excitation and generate good SERS performance using a lower level of laser power. Interestingly, UC materials can convert two or more low-energy pump photons to a higher-energy output photon,[15,16] which offers the possibility of overcoming the problems mentioned.

Recently, the coupling of upconversion (UC) nanocrystals (NCs) with noble metal nanoparticles such as Ag and Au has become a valuable strategy for improving their luminescence.[17,18] The intrinsic mechanism might be similar to that involved in LSPR-related Raman enhancement. However, few examples of UC material-related SERS have been reported and the mechanism remains unclear.

Institute of Intelligent Machines, Chinese Academy of Science, Hefei, China. E-mail: hlliu@iim.ac.cn; lbyang@iim.ac.cn; Fax: +86-551-6559-2420; Tel: +86-551-6559-2385

† Electronic supplementary information (ESI) available. See DOI: 10.1039/c4an01202j

In the present article we speculate that the incorporation of UC materials into SERS-active nanoparticles might shed new light on the role of UC materials in Raman enhancement and plasmon photocatalysis. As shown in Scheme 1, under NIR excitation at 785 nm, Yb^{3+} ions act as sensitizers and are primary absorbers of the NIR excitation. Yb^{3+} then transfers the energy absorbed from NIR excitation to Er^{3+}, and the Er^{3+} ions are excited from the $^4I_{15/2}$ ground state to the $^4I_{11/2}$ excited state by $Yb^{3+} \rightarrow Er^{3+}$ energy transfer. The luminescent states of Er^{3+} are excited by two consecutive $Yb^{3+} \rightarrow Er^{3+}$ energy transfer events, the first taking place in the $^4I_{15/2}$ ground state, and the second is a long-lived intermediate excited state ($^4I_{13/2}$ or $^4I_{11/2}$). The Er^{3+} ion is then excited to the $^4F_{7/2}$ state by a second $Yb^{3+} \rightarrow Er^{3+}$ energy transfer, after which the Er^{3+} ion decays non-radiatively to the $^2H_{11/2}$, $^4S_{3/2}$ and $^4F_{9/2}$ levels. This gives a dominant green luminescence ($^2H_{11/2} \rightarrow {}^4I_{15/2}$, $^4S_{3/2} \rightarrow {}^4I_{15/2}$), and red emission is obtained by the transition $^4F_{9/2} \rightarrow {}^4I_{15/2}$ (shown in the inset in Fig. 1(B)).[19–22]

In noble metal NPs such as Au or Ag NPs, the broad absorption of the noble metals can increase the power of excitation by local field enhancement, resulting in an increase in excited Yb^{3+} ions and greater energy transfer from excited Yb^{3+} to Er^{3+}.[23] The highly enhanced local field density will act on the SERS effects, resulting in dramatically increased plasmon photocatalysis. In addition, the UC emissions convert the NIR radiation into green emission, with bands at 520, 528 and 540 nm, which are close to the LSPR peak of Ag, resulting in significantly increased EM fields at the noble metal surface and amplification of the Raman scattering. This analysis is nicely supported by the excellent improvement of Raman enhancement and photocatalytic ability in the following experiments.

2. Experimental

2.1 Chemicals and materials

Silver nitrate ($AgNO_3$), sodium citrate, *p*-aminothiophenol (pATP), NaF, $ErCl_3$, $YbCl_3 \cdot 6H_2O$, $YCl_3 \cdot 6H_2O$ and ethylene diamine tetra-acetic acid (EDTA), were all AR grade and

Published on 10 September 2014. Downloaded by Hefei Institutes of Physical Science, Chinese Academy of Sciences on 04/12/2014 00:43:01.

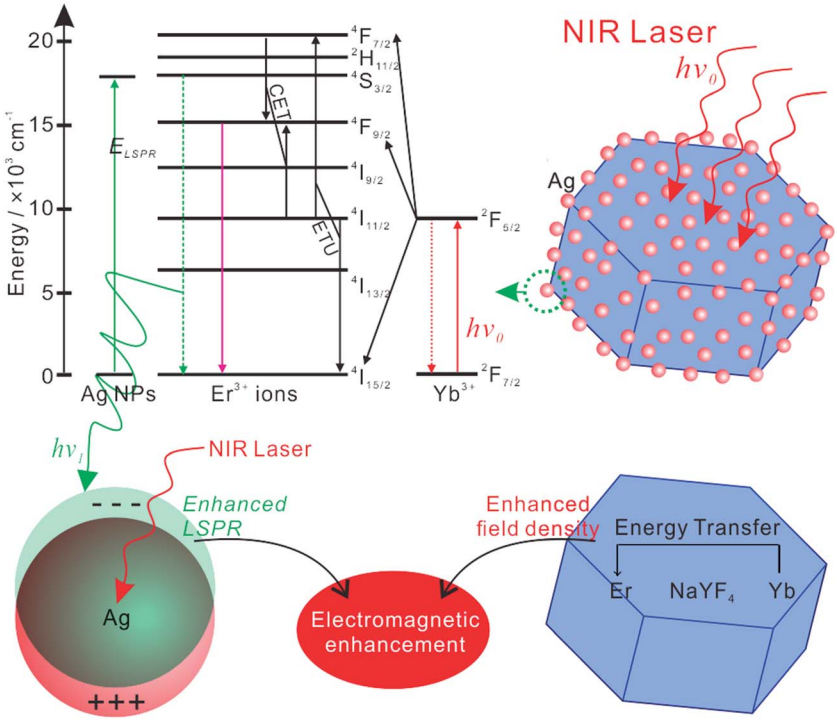

Scheme 1 Illustration of the relevant processes of energy transfer in UC@Ag particles and the LSPR, enhanced by the LSPR of Ag NPs. ETU: energy transfer upconversion; CET: co-operative energy transfer.

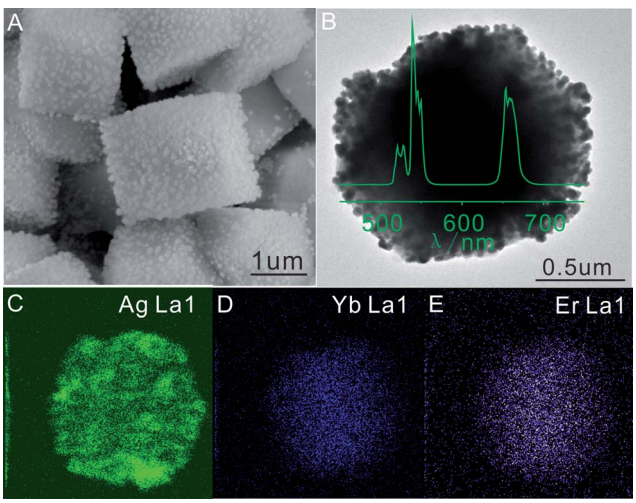

Fig. 1 (A) SEM and (B) TEM images of UC@Ag (inset: the corresponding emission spectrum); and (C–E) the elemental mapping of a single particle of UC@Ag from the HRTEM images, based on Ag La1, Yb La1 and Er La1.

obtained from Shanghai Reagent Co. They were used without further purification. Solutions were prepared in distilled water without pH regulation. The experiments were carried out at room temperature (25 °C) in unbuffered water.

2.2 Synthesis of upconversion material

$NaYF_4$:Yb,Er NCs were synthesized by a simple hydrothermal method using trisodium citrate as capping agent.[1] An aqueous solution of $YCl_3 \cdot 6H_2O$, $YbCl_3 \cdot 6H_2O$ and $ErCl_3$ (lanthanide ion molar ratio, Y : Yb : Er = 88 : 10 : 2) was mixed with an aqueous solution of trisodium citrate with vigorous stirring, resulting in a white complex. An aqueous solution of NaF was then added to the complex and stirred for 1 h. The newly formed complex precursor solution was then transferred to a 60 mL autoclave and heated at 180 °C for 3 h. The $NaYF_4$:Yb,Er NCs were separated by centrifugation and rinsed a number of times in ultrapure water.

2.3 Ag coating of the upconversion material

Ag NCs attached to $NaYF_4$:Yb,Er NCs were prepared using trisodium citrate as coupling agent and reductant. The dried $NaYF_4$:Yb,Er NCs were redispersed in ultrapure water and $AgNO_3$ solution added, and the combined solution was stirred and heated at 100 °C. Trisodium citrate solution was added to the solution, which was held at the boil for 1 h. The products obtained were precipitated by centrifugation and rinsed several times with ultrapure water.

2.4 Synthesis of Ag NPs

Ag NPs were prepared by citrate reduction of $AgNO_3$.[2] 1 mL 0.1 M $AgNO_3$ was added to 99 mL ultrapure water and the solution heated to the boil under reflux. 10 g L^{-1} trisodium citrate solution (4 mL) was then added rapidly and the temperature kept at this level for 1 h. The products obtained were precipitated by centrifugation and rinsed thoroughly with ultrapure water.

This journal is © The Royal Society of Chemistry 2014

Published on 10 September 2014. Downloaded by Hefei Institutes of Physical Science, Chinese Academy of Sciences on 04/12/2014 00:43:01.

2.5 Apparatus

Scanning electron microscope (SEM) images were recorded using a Sirion 200 field-emission SEM. X-ray scattering patterns of the powder samples were produced on a Philips X-Pert Pro X-ray diffractometer (XRD) with Cu-Kα radiation. Transmission electron microscope (TEM) images were recorded at an acceleration voltage of 200 kV using a JEOL 2010 high-resolution TEM equipped with X-ray energy dispersive spectroscopy (EDS) capability.

UC luminescence spectra were recorded using a fluorescence spectrophotometer with 980 nm laser. Raman spectra were carried out on a LabRAM HR800 confocal microscope Raman system (Horiba Jobin Yvon), using an Ar ion laser at 785 nm and approximately 1 mW. All the spectra reported were the result of a single 1 s accumulation.

3. Results and discussion

Hexagonal $NaYF_4$:Yb,Er microcrystals of uniform size and shape, average side length ~600 nm, were successfully synthesized by a simple hydrothermal method. A straightforward procedure was developed to decorate high-density Ag NPs on the surface of the microcrystals (Fig. 1(A) and (B)).

Single particles of $NaYF_4$:Yb,Er@Ag microcrystals (labeled UC@Ag) were used to investigate their Raman enhancement and plasmon photocatalysis behaviour under NIR excitation at relatively low laser power. The HRTEM at high-angle annular dark field showed that the elements Ag, Yb or Er were distributed throughout the entire particle (Fig. 1). The diameters of the Ag NPs were mainly within the range 45 ± 13 nm (ESI Fig. S3A†). The LSPR peak of the Ag NPs decorated on $NaYF_4$:Yb,Er was at ~405 nm, and there was no red shift affecting the broad absorption of UC (ESI Fig. S3B and C†). For reference the closely packed multilayer of pure Ag nanoparticles (labelled ML-Ag) were measured, and the inter-particle gap between the particles was shown to be below 5 nm (ESI Fig. S4A and B†), maximizing the local electric field and greatly amplifying the Raman signals of the target molecules.[24,25]

In contrast, the distribution of the Ag NPs decorated on $NaYF_4$:Yb,Er microcrystals was relatively sparse (Fig. 1(A) and (B)) and the interparticle gap was much greater than that for ML-Ag. Due to the limitations of our SERS experimental set-up, a 785 nm laser was selected as the excitation source.

To verify the SERS capability of UC@Ag, a series of experiments were carried out using pATP as the signal reporter under a 785 nm excitation laser.[26] We first demonstrated that the pATP absorbed was transformed to DMAB under a high-power laser, and the Raman signals of the b_2 modes were actually supplemented by the a_g mode of DMAB. As shown in Fig. 2(B), the intensity of the 1142 cm^{-1} peak produced by the ML-Ag was only about 700 cnts. The corresponding SERS intensity of the 1142 cm^{-1} peak of pATP adsorbed on UC@Ag was about 35 000 cnts, as shown in Fig. 2(A), nearly 50 times greater than that obtained on ML-Ag.

As mentioned above, the shape, LSPR and size of the Ag NPs decorated on $NaYF_4$:Yb,Er were similar to those of pure Ag NPs.

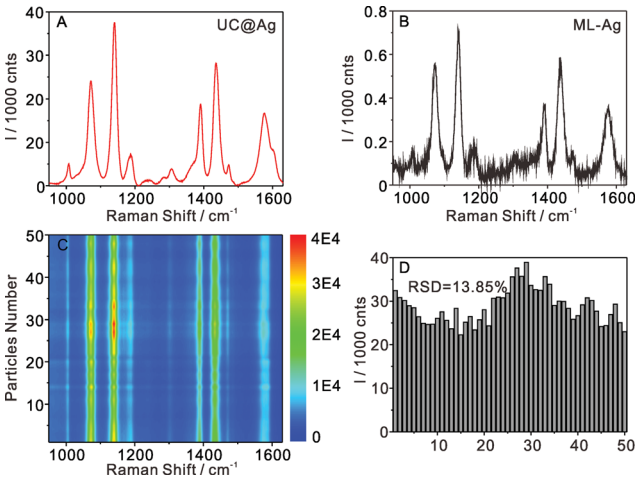

Fig. 2 SERS spectra of 10^{-6} M pATP adsorbed on (A) a single particle of UC@Ag, and (B) the ML-Ag, with an excitation laser of 785 nm and integration time of 5 s; (C) a series of SERS spectra of 10^{-6} M pATP molecules collected on 50 randomly selected particles of the UC@Ag; and (D) the intensities at 1142 cm^{-1} of pATP.

More importantly, the interparticle gaps among the Ag NPs decorated on $NaYF_4$:Yb,Er were larger than those of the ML-Ag, confirming that the Ag NPs modified on $NaYF_4$:Yb,Er cannot enhance by one order of magnitude the SERS intensity of analyte in comparison to ML-Ag. It is therefore the presence of UC materials that contributes to the greatly improved SERS performance of UC@Ag, as illustrated in Scheme 1. The intensity of the main vibration of pATP from 50 particles of SERS data shown in Fig. 2(C) indicates excellent reproducibility, further confirmed by the relative standard deviation of the Raman intensity of 1142 cm^{-1} (Fig. 2(D)).[11] Different batches of SERS substrate also indicated good reproducibility (ESI Fig. S5†).

To demonstrate the sensitivity of the UC@Ag substrate, SERS spectra of pATP were collected by varying the concentration between 10^{-5} and 10^{-9} M, as shown in Fig. 3(A). The intensity of the strongest peak at 1142 cm^{-1} was used for quantitative evaluation of the detection level and exhibited a good linear relationship for concentrations ranging from 1.0×10^{-5} to 1.0×10^{-9} M ($R^2 = 0.98$), as shown in Fig. 3(D). The limit of detection was 1.0×10^{-9} M, determined from three standard deviations above the background. For comparison, Fig. 3(C) shows the SERS spectra of pATP at different concentrations, also collected on ML-Ag. Also shown in Fig. 3(D), the Raman intensity at 1142 cm^{-1} with the logarithm of pATP concentration can be well fitted by a linear plot ($R^2 = 0.99$). The limit of detection was determined as 5.0×10^{-7} M, from three standard deviations above the background, and the sensitivity of UC@Ag substrate was thus about three orders of magnitude lower than that of the ML-Ag substrate.

Although we recognized the consistency of the Ag particles on the two SERS substrates, the comparison of SERS enhancement between the two substrates remained unconvincing. The SERS enhancement effect of a fixed position on the same substrate was examined under two different excitation lasers, at 785 nm and 532 nm. A similar area of UC@Ag substrate excited

Published on 10 September 2014. Downloaded by Hefei Institutes of Physical Science, Chinese Academy of Sciences on 04/12/2014 00:43:01.

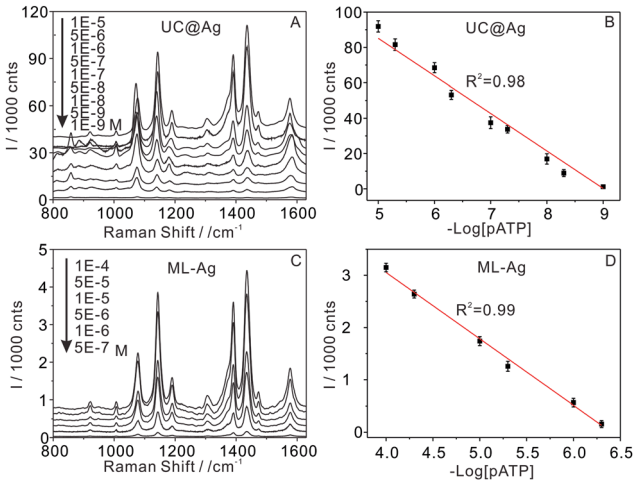

Fig. 3 SERS spectra obtained at different concentrations of pATP using (A) UC@Ag, and (C) ML-Ag substrates under 785 nm; (B) and (D) are the linear correlation of Raman intensity at 1142 cm^{-1} with the logarithm of pATP concentration.

by the two lasers exhibited different degrees of SERS enhancement (Fig. 4(A) and (B)). The excitation laser at 785 nm produced a strong SERS signal, with a maximum strength of 23 000 cnts at 1072 cm^{-1} (curve (b) in Fig. 4(A)). In contrast, the excitation laser of 532 nm produced a much stronger SERS signal, with a maximum strength of 47 000 cnts at 1072 cm^{-1} (curve (a) in Fig. 4(A)). The laser wavelength-dependent enhancement sensitivity (Es) can be estimated by comparison of the intensity of the 1072 cm^{-1} band, using eqn (1):

$$Es = I/(C \times M), \quad (1)$$

where I is the intensity of pATP, C the concentration of pATP, and M is the quantity of the substrates; in two different experiments C and M were identical.[27] It can be estimated that the enhancement effect of 532 nm is only about 2.1 times that of 785 nm on the UC@Ag substrate (Fig. 4(B)).

Similarly, the enhancement effect of ML-Ag under two excitation lasers, at 785 nm and 532 nm, was also examined. Fig. 4(C) shows that the excitation laser at 785 nm produced a relatively weak SERS signal, of maximum strength 700 cnts at 1072 cm^{-1} (curve (b) in Fig. 4(C)). In contrast, the excitation laser at 532 nm produced a much stronger SERS signal, with a maximum strength of 14 000 cnts at 1072 cm^{-1} (curve (a) in Fig. 4(C)). Hence, it can also be estimated that the enhancement effect at 532 nm was about 20 times that at 785 nm on ML-Ag

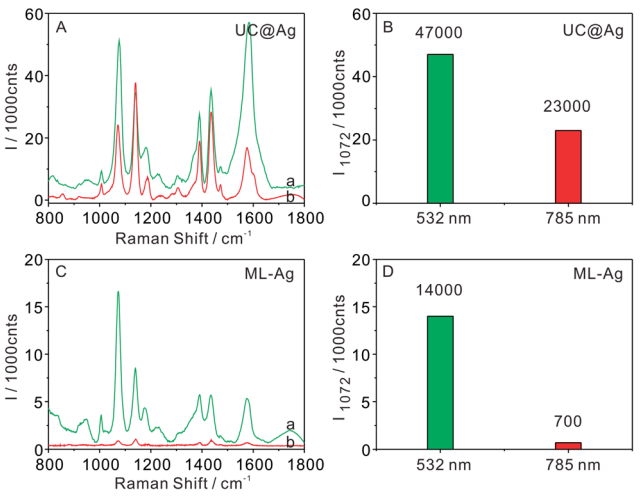

Fig. 4 (A) The SERS spectra of 10^{-6} M pATP on UC@Ag at (a) 532 nm and (b) 785 nm; (B) comparison of the enhancement effect of the two excitation lasers; (C) the SERS spectra of 10^{-6} M pATP on ML-Ag at (a) 532 nm and (b) 785 nm; and (D) comparison of enhancement effect of the two excitation lasers.

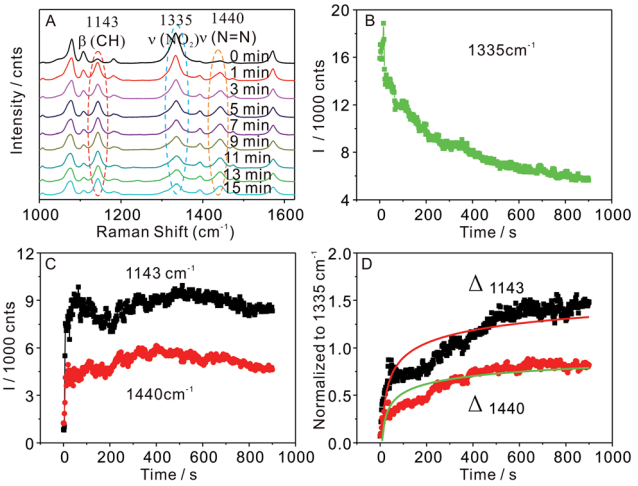

Fig. 5 (A) Time-dependent SERS spectra of pNTP under continuous exposure to a 785 nm laser. The spectra were collected on UC@Ag particles, with an integration time of 2 s; (B) time-dependent Raman illumination intensities of the peaks at 1335, and (C) at 1143 and 1440 cm^{-1}; and (D) illumination time-dependent relative Raman intensities of the peaks at 1143 and 1440 cm^{-1}, normalized by the intensities at the 1335 cm^{-1} peak.

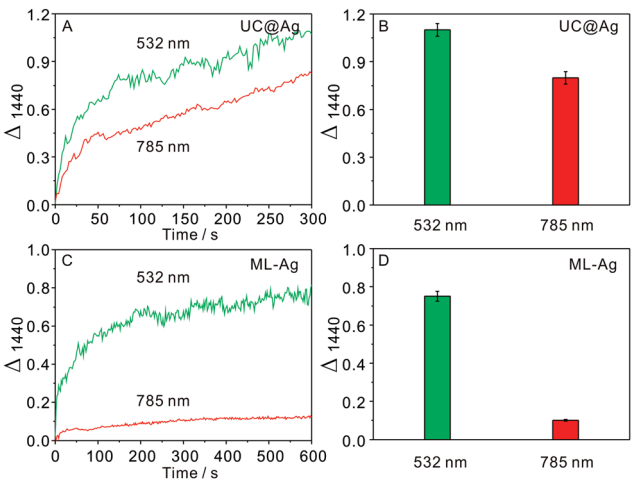

Fig. 6 The Δ_{1440} curves under continuous exposure to the lasers at 532 nm and 785 nm on (A) and (B) UC@Ag, and (C) and (D) ML-Ag. The error bars represent the standard deviation between three sets of time-course SERS mappings.

This journal is © The Royal Society of Chemistry 2014

Published on 10 September 2014. Downloaded by Hefei Institutes of Physical Science, Chinese Academy of Sciences on 04/12/2014 00:43:01.

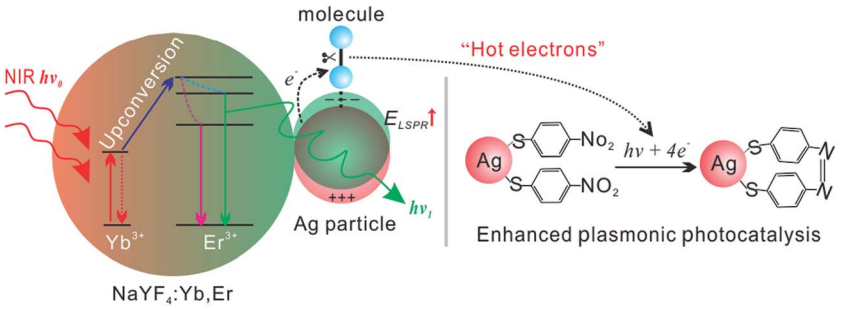

Scheme 2 Schematic illustration of the plasmon-driven dimerization of pNTP into DMAB on UC@Ag.

(Fig. 4(D)). These relative comparisons indicated that the presence of UC materials improved the SERS enhancement by almost one order of magnitude under an excitation laser at 785 nm.

Enhancement of the SERS intensities is particularly to be anticipated if there is a greater increase in the number of adsorbed analyte molecules on UC@Ag than on the ML-Ag substrate for a given cross-section. However, this possibility may be discounted on examining the relative variations in peak intensities in a plasmon-driven chemical reaction. A number of recent research results have clearly demonstrated the promising potential of surface plasmon used as a novel "catalytic" medium for understanding possible chemical reactions induced by laser excitation.[28,29]

Within the context described above, the plasmonic photocatalysis of pNTP dimerizing into DMAB was investigated on single particles of UC@Ag and the ML-Ag substrate. A time-course SERS mapping was performed on a single particle of UC@Ag under continuous exposure to a 785 nm laser (Fig. 5). As the exposure time increased, the SERS intensity of the $\nu(NO_2)$ stretching mode at 1335 cm^{-1} decreased dramatically (Fig. 5(A) and (B)). The peaks at 1385 and 1440 cm^{-1}, attributed to the ν(N=N) stretching mode, and at 1143 cm^{-1}, attributed to the β(CH) stretching mode of DMAB, gradually increased (Fig. 5(C)), which was not observed in a normal Raman spectrum (ESI Fig. S7†).[28] This increase indicated the dimerizing of pNTP molecules into DMAB. It is worth mentioning that the intensities of ν(N=N) and β(CH) decreased slightly after about 500 s exposure (Fig. 5(C)). The whole measuring process took more than 10 min, and a long exposure time may therefore cause the signal attenuation and local alteration in the structure of the substrate. Fig. 5(D) shows the illumination time dependence of the relative intensities of the 1143 and 1440 cm^{-1} peaks normalized by the 1335 cm^{-1} peak, according to eqn (2):

$$\Delta_i = I_i/I_{1335}, \quad (2)$$

where I is the value of the peak intensity. The ratio Δ_{1440} can in some degree represent the apparent conversion rate of pNTP into DMAB.

Similarly, time-course SERS mapping was also performed under similar conditions on single particles of UC@Ag under continuous exposure to a 532 nm laser (ESI Fig. S8†). After about 300 s illumination, Δ_{1440} under the laser at 532 nm reached a relatively stable value in the region of 1.1, and the laser at 785 nm produced a lower value of about 0.8 (Fig. 6(B)). It was estimated that the Δ_{1440} of 532 nm was only about 1.38 times that of 785 nm on the UC@Ag particles. To corroborate the enhanced photocatalysis on UC@Ag, plasmon-driven photocatalysis was also investigated on the ML-Ag substrate under the excitation lasers at 532 nm and 785 nm. Fig. 6(C) illustrates that the stable Δ_{1440} excited under the 532 nm laser was about 0.75, whereas that under the 785 nm laser was only about 0.1. It can thus also be estimated that the Δ_{1440} of 532 nm was about 7.5 times that of 785 nm on ML-Ag substrate (Fig. 6(D)). The ratios of the apparent conversion rate on the same substrate discount the effect of concentration of the adsorbed molecules and other negative effects.

The origin of the difference in Raman enhancement and conversion rate between UC@Ag and ML-Ag during photocatalysis is a matter of speculation. The presence of UC materials might provide more excitation lines and a much stronger plasmon resonance. The stronger LSPR produces a higher density of "hot" electrons, and this can boost the chemical reaction (Scheme 2). Furthermore, the "hot" electrons of high kinetic energy above the Fermi level may jump to the unoccupied resonance energy level of chemical reactants near the metal surface and transfer to the intra-molecular vibrational energy during the interactions.[30] In both cases the energy barrier of the chemical reactions would be reduced.[31] At present, we have concluded that UC serves as a light converter to upconvert the NIR light into a visible condition, and high plasmon resonance is induced since the LSPR of Ag NPs lies within the visible range. In addition, the energy transfer from excited Yb^{3+} to Er^{3+} in UC will increase the local field density, and this induces a plasmon field enhancement effect. Both of these effects will influence SERS performance, resulting in significantly improved Raman enhancement and plasmon photocatalytic ability.

4. Conclusions

The UC material has for the first time been successfully incorporated into SERS-active substrates. This has demonstrated that a low-power NIR laser can give excellent signals on UC@Ag, in comparison with conventional SERS measurements on pure Ag substrates. Furthermore, electron transitions in UC particles produce strong plasmon resonances, which boost the chemical

Published on 10 September 2014. Downloaded by Hefei Institutes of Physical Science, Chinese Academy of Sciences on 04/12/2014 00:43:01.

reaction, and perfect plasmon photocatalytic ability was obtained under NIR excitation at relatively low laser power. The NIR excitation of the UC@Ag substrate provided a deeper penetration depth at lower power, opening up a new application field for UC-noble metal composites, particularly in biological applications. In addition, a new research direction has now been revealed for the synthesis and applications of SERS-active nanostructures.

Acknowledgements

This study was supported by the National Basic Research Program of China (2011CB933700), the National Instrumentation Program of China (2011YQ0301241001 and 2011YQ0301241101), the National Natural Science Foundation of China (21305142, 61273066 and 11205204), and the Natural Science Foundation of Anhui Province, China (1308085QB27).

References

1 H. L. Liu, Z. L. Yang, L. Y. Meng, Y. D. Sun, J. Wang, L. B. Yang, J. H. Liu and Z. Q. Tian, *J. Am. Chem. Soc.*, 2014, **136**, 5332–5341.
2 J. A. Dougan and K. Faulds, *Analyst*, 2012, **137**, 545–554.
3 J. F. Li, Y. F. Huang, Y. Ding, Z. L. Yang, S. B. Li, X. S. Zhou, F. R. Fan, W. Zhang, Z. Y. Zhou, D. Y. Wu, B. Ren, Z. L. Wang and Z. Q. Tian, *Nature*, 2010, **464**, 392–395.
4 W. Xie, C. Herrmann, K. Kompe, M. Haase and S. Schlucker, *J. Am. Chem. Soc.*, 2011, **133**, 19302–19305.
5 M. Grabiec, A. Wolak, O. Veron, J. P. Blondeau, N. Pellerin, M. Allix, S. Pellerin and K. Dzierzega, *Plasmonics*, 2012, **7**, 279–286.
6 Y. M. Ma, H. L. Liu, K. Qian, L. B. Yang and J. H. Liu, *J. Colloid Interface Sci.*, 2012, **386**, 451–455.
7 Y. W. Zhang, S. Liu, L. Wang, X. Y. Qin, J. Q. Tian, W. B. Lu, G. H. Chang and X. P. Sun, *RSC Adv.*, 2012, **2**, 538–545.
8 A. D. McFarland, M. A. Young, J. A. Dieringer and R. P. Van Duyne, *J. Phys. Chem. B*, 2005, **109**, 11279–11285.
9 J. Zhao, J. A. Dieringer, X. Y. Zhang, G. C. Schatz and R. P. Van Duyne, *J. Phys. Chem. C*, 2008, **112**, 19302–19310.
10 Y. M. Ma, Q. Q. Ding, L. B. Yang, L. Zhang and Y. H. Shen, *Appl. Surf. Sci.*, 2013, **265**, 346–351.
11 H. L. Liu, Y. D. Sun, Z. Jin, L. B. Yang and J. H. Liu, *Chem. Sci.*, 2013, **4**, 3490–3496.
12 B. Crisan, O. Soritau, M. Baciut, R. Campian, L. Crisan and G. Baciut, *Part. Sci. Technol.*, 2013, **31**, 168–173.
13 A. Lee, G. F. S. Andrade, A. Ahmed, M. L. Souza, N. Coombs, E. Tumarkin, K. Liu, R. Gordon, A. G. Brolo and E. Kumacheva, *J. Am. Chem. Soc.*, 2011, **133**, 7563–7570.
14 H. C. Jeon, C. J. Heo, S. Y. Lee and S. M. Yang, *Adv. Funct. Mater.*, 2012, **22**, 4268–4274.
15 F. Wang, Y. Han, C. S. Lim, Y. H. Lu, J. Wang, J. Xu, H. Y. Chen, C. Zhang, M. H. Hong and X. G. Liu, *Nature*, 2010, **463**, 1061–1065.
16 F. Wang, D. Banerjee, Y. S. Liu, X. Y. Chen and X. G. Liu, *Analyst*, 2010, **135**, 1839–1854.
17 J. C. Goldschmidt, S. Fischer, H. Steinkemper, F. Hallermann, G. von Plessen, K. W. Kramer, D. Biner and M. Hermle, *IEEE J. Photovoltaics*, 2012, **2**, 134–140.
18 W. Feng, L. D. Sun and C. H. Yan, *Chem. Commun.*, 2009, 4393–4395.
19 S. Schietinger, T. Aichele, H. Q. Wang, T. Nann and O. Benson, *Nano Lett.*, 2010, **10**, 134–138.
20 H. P. Paudel, L. L. Zhong, K. Bayat, M. F. Baroughi, S. Smith, C. K. Lin, C. Y. Jiang, M. T. Berry and P. S. May, *J. Phys. Chem. C*, 2011, **115**, 19028–19036.
21 J. H. Wu, J. L. Wang, J. M. Lin, Z. Lan, Q. W. Tang, M. L. Huang, Y. F. Huang, L. Q. Fan, Q. B. Li and Z. Y. Tang, *Adv. Energy Mater.*, 2012, **2**, 78–81.
22 T. Jiang, Y. Liu, S. S. Liu, N. Liu and W. P. Qin, *J. Colloid Interface Sci.*, 2012, **377**, 81–87.
23 N. Liu, W. P. Qin, G. S. Qin, T. Jiang and D. Zhao, *Chem. Commun.*, 2011, **47**, 7671–7673.
24 M. Rycenga, C. M. Cobley, J. Zeng, W. Y. Li, C. H. Moran, Q. Zhang, D. Qin and Y. N. Xia, *Chem. Rev.*, 2011, **111**, 3669–3712.
25 S. M. Stranahan, E. J. Titus and K. A. Willets, *ACS Nano*, 2012, **6**, 1806–1813.
26 H. L. Liu, L. B. Yang, H. W. Ma, Z. M. Qi and J. H. Liu, *Chem. Commun.*, 2011, **47**, 9360–9362.
27 B. H. Liu, G. M. Han, Z. P. Zhang, R. Y. Liu, C. L. Jiang, S. H. Wang and M. Y. Han, *Anal. Chem.*, 2012, **84**, 255–261.
28 L. L. Kang, P. Xu, B. Zhang, H. H. Tsai, X. J. Han and H. L. Wang, *Chem. Commun.*, 2013, **49**, 3389–3391.
29 B. Dong, Y. R. Fang, X. W. Chen, H. X. Xu and M. T. Sun, *Langmuir*, 2011, **27**, 10677–10682.
30 J. Yang, D. Wang, H. Han and C. Li, *Acc. Chem. Res.*, 2013, **46**, 1900–1909.
31 M. T. Sun, Z. L. Zhang, H. R. Zheng and H. X. Xu, *Sci. Rep.*, 2012, **2**(1–4), 647.

 This journal is © The Royal Society of Chemistry 2014